Geosci. Model Dev. Discuss., doi:10.5194/gmd-2016-49, 2016
Manuscript under review for journal Geosci. Model Dev.
Published: 15 April 2016

Geoscientific Model Development Discussions
Open Access
EGU

Simple Process-Led Algorithms for Simulating Habitats (SPLASH v.1.0): Robust Indices of Radiation, Evapotranspiration and Plant-Available Moisture

Tyler W. Davis[1,2], I. Colin Prentice[2,3,4,5], Benjamin D. Stocker[2], Rhys J. Whitley[3,5], Han Wang[3,4], Bradley J. Evans[5,6], Angela V. Gallego-Sala[7], Martin T. Sykes[8], and Wolfgang Cramer[9]

[1]United States Department of Agriculture-Agricultural Research Service, Robert W. Holley Center for Agriculture and Health, Ithaca, United States
[2]AXA Chair of Biosphere and Climate Impacts, Grand Challenges in Ecosystems and the Environment and Grantham Institute - Climate Change and the Environment, Department of Life Sciences, Imperial College London, Silwood Park Campus, Ascot, United Kingdom
[3]Department of Biological Sciences, Macquarie University, North Ryde, New South Wales, Australia
[4]State Key Laboratory of Soil Erosion and Dryland Farming on the Loess Plateau, College of Forestry, Northwest Agriculture & Forestry University, Yangling 712100, China
[5]Terrestrial Ecosystem Research Network (TERN) Ecosystem Modelling and Scaling Infrastructure (eMAST), Sydney, New South Wales, Australia
[6]Faculty of Agriculture and Environment, Department of Environmental Sciences, The University of Sydney, Sydney, New South Wales, Australia
[7]Department of Geography, University of Exeter, Exeter, Devon, United Kingdom
[8]Department of Physical Geography and Ecosystem Science, Lund University, Lund, Sweden
[9]Mediterranean Institute of marine and terrestrial Biodiversity and Ecology (IMBE), Aix Marseille University, CNRS, IRD, Avignon University, Aix-en-Provence, France

Correspondence to: I. Colin Prentice (c.prentice@imperial.ac.uk)

Abstract. Bioclimatic indices for use in studies of ecosystem function, species distribution, and vegetation dynamics under changing climate scenarios depend on estimates of surface fluxes and other quantities, such as radiation, evapotranspiration and soil moisture, for which direct observations are sparse. These quantities can be derived indirectly from meteorological variables, such as air temperature, precipitation and cloudiness. Here we present a consolidated set of Simple Process-Led Algorithms for Simulating Habitats (SPLASH) allowing robust approximations of key quantities at ecologically relevant time scales. We specify equations, derivations, simplifications and assumptions for the estimation of daily and monthly quantities of top-of-the-atmosphere solar radiation, net surface radiation, photosynthetic photon flux density, evapotranspiration (potential, equilibrium and actual), condensation, soil moisture, and runoff, based on analysis of their relationship to fundamental climatic drivers. SPLASH, as presented here, is designed for application at discrete locations; however, the same methodology can naturally be applied to spatial grids. The climatic drivers include a minimum of three meteorological inputs: precipitation, air temperature, and either fraction of bright sunshine hours or fractional cloud cover. Indices, such as the moisture index, the climatic water deficit, and the Priestley-Taylor coefficient, are also defined. The SPLASH code is transcribed in C++, FORTRAN, Python, and R. One year of results from a specific location are provided to exemplify the daily and monthly model outputs, following a two-year spin-up of soil moisture content.

Geosci. Model Dev. Discuss., doi:10.5194/gmd-2016-49, 2016
Manuscript under review for journal Geosci. Model Dev.
Published: 15 April 2016

Geoscientific Model Development Discussions
Open Access
EGU

1 Introduction

Despite the existence of dense networks of meteorological monitoring stations around the world, plant ecophysiology and biogeography suffer from a lack of globally distributed observational data, especially those central to the estimation of ecosystem-level photosynthesis, including photosynthetic photon flux density and soil moisture. To overcome this deficiency, we present Simple Process-Led Algorithms for Simulating Habitats (SPLASH) for generating driving datasets for ecological and land-surface models from more readily available meteorological observations.

SPLASH is a continuation of the STASH (STAtic SHell) model, which was originally developed for modeling the climatic controls on plant species distributions at a regional scale (Sykes and Prentice, 1995, 1996; Sykes et al., 1996). The intention of STASH was to provide bioclimatic indices, reflecting the environment experienced by plants more closely than either standard summary variables such as mean annual temperature, or such constructions as 'mean precipitation of the warmest quarter,' while requiring only standard meteorological data as input. A key component of STASH was a simple, physically-based soil moisture accounting scheme, first developed by Cramer and Prentice (1988), which has been used *inter alia* in the original, highly cited BIOME model (Prentice et al., 1992); the general forest succession model (FORSKA) described by Prentice et al. (1993); and the Simple Diagnostic Biosphere Model (Knorr and Heimann, 1995). Despite the subsequent development of more complex Dynamic Global Vegetation Models (Cramer et al., 2001; Sitch et al., 2003; Woodward and Lomas, 2004; Quillet et al., 2010; Prentice and Cowling, 2013; Fisher et al., 2014) and Land Surface Models, the relatively simple algorithms in STASH continue to have many applications, including to new areas such as the distribution of plant functional traits (Harrison et al., 2010; Meng et al., 2015), assessment of climate-change impacts on specific biomes (Gallego-Sala and Prentice, 2012), large-scale water resources assessments (e.g. Ukkola et al., 2015) and simple first-principles modeling of primary production (Wang et al., 2014). The continuing utility of these algorithms owes much to their robustness, which in turn depends on the implicit assumption that vegetation functions predictably—so that, for example, evapotranspiration occurs at a potential rate under well-watered conditions, and is reduced as soil water is drawn down. STASH is thus unsuitable to answer questions like the effect of imposed vegetation changes on runoff, or modeling vegetation-atmosphere feedbacks. Much more complex models that dynamically couple soil, vegetation and atmospheric boundary layer processes exist for such applications; however, their complexity brings a burden in terms of lack of robustness and, potentially, large inter-model differences (Prentice et al., 2014).

Despite their long history of use, no single publication documents the algorithms of the STASH model. This work aims to fill that gap to allow for the continued development and use of these algorithms. As the new incarnation of STASH, SPLASH provides the same physically-based soil moisture accounting scheme with updated and corrected analytical expressions for the calculation of daily radiation, evapotranspiration, and soil moisture. Included in this documentation are the equation derivations, variable definitions, and information regarding model assumptions and limitations. One notable improvement is that we have discontinued the approximation of constant angular velocity in the orbit of Earth around the Sun. This version is thus suitable for palaeoclimate applications, whereby orbital precession (as well as changes in obliquity and eccentricity) influences the seasonal distribution of insolation. SPLASH also includes explicit consideration of elevation effects on biophysical quantities.

Geosci. Model Dev. Discuss., doi:10.5194/gmd-2016-49, 2016
Manuscript under review for journal Geosci. Model Dev.
Published: 15 April 2016

Geoscientific Model Development Discussions

Key model outputs include daily insolation (incoming solar radiation at the top of the atmosphere) and net surface radiation (H_o and H_N, respectively); daily photosynthetic photon flux density (Q_n); daily condensation, soil moisture and runoff (C_n, W_n, and RO); and daily equilibrium, potential and actual evapotranspiration (E_n^q, E_n^p, and E_n^a). Unlike the STASH model, SPLASH explicitly distinguishes potential and equilibrium evapotranspiration, recognizing that under well-watered conditions the excess of the former over the latter is a requirement for foliage to be cooler than the surrounding air, as has long been observed under high environmental temperatures (e.g. Linacre, 1967).

Input values of latitude, ϕ (rad), elevation, z (m), mean daily air temperature, T_{air} (°C), and fractional hours of bright sunshine, S_f (unitless), are necessary for calculating the daily quantities of net radiation and evapotranspiration. Daily observed precipitation, P_n ($\mathrm{mm\,d^{-1}}$), is necessary for updating daily soil moisture. T_{air} and P_n may be derived from various sources, including the freely available daily-averaged air temperature and precipitation reanalysis data from the Water and Global Change (WATCH) program's meteorological forcing data set (Weedon et al., 2014). Cloud cover fraction, for example the simulated quantities given in the CRU TS3.21 dataset (Harris et al., 2014), may be used to approximate S_f. Penman's one-complement approximation based on the cloudiness fraction is regarded here as a sufficient estimate of S_f (Penman, 1948). The piecewise linear method of Hulme et al. (1995)—an adaptation of the Doorenbos-Pruitt estimation procedure (Doorenbos and Pruitt, 1977)—as used in the development of the CRU cloudiness climatology (New et al., 1999) gives similar results.

We present SPLASH comprehensively re-coded in a modular framework to be readable, understandable and reproducible. To facilitate varied application requirements (including computational speed), four versions of the code (C++, FORTRAN, Python, and R) are available in an online repository (see Code Availability). The algorithms as presented here focus on application to individual site locations, but a natural extension is towards spatially distributed grid-based datasets.

In line with the intention of the original STASH algorithms, we also present bioclimatic indices at the monthly and annual timescales to exemplify the analytical applications of the SPLASH model outputs.

2 Methodology

The implementation of the soil-moisture accounting scheme follows the steps outlined by Cramer and Prentice (1988), where daily soil moisture, W_n (mm), is calculated based on the previous day's moisture content, W_{n-1}, incremented by daily precipitation, P_n ($\mathrm{mm\,d^{-1}}$), and condensation, C_n ($\mathrm{mm\,d^{-1}}$), and reduced by daily actual evapotranspiration, E_n^a ($\mathrm{mm\,d^{-1}}$):

$$W_n = W_{n-1} + P_n + C_n - E_n^a, \tag{1}$$

where P_n is a model input, C_n is estimated based on the daily negative net radiation, and is the analytical integral of the minimum of the instantaneous evaporative supply and demand rates over a single day. An initial condition of W_n is assumed between zero and the maximum soil moisture capacity, W_m (mm), for a given location and is equilibrated over an entire year by successive model iterations (i.e., model spin-up).

To solve the simple 'bucket model' represented by Eq. 1, the following steps are taken at the daily timescale: calculate the radiation terms, estimate the condensation, estimate the evaporative supply, estimate the evaporative demand, calculate the

Geosci. Model Dev. Discuss., doi:10.5194/gmd-2016-49, 2016
Manuscript under review for journal Geosci. Model Dev.
Published: 15 April 2016

Geoscientific Model Development Discussions

actual evapotranspiration, and update the daily soil moisture. Daily quantities may be aggregated into monthly and annual totals and used in moisture index calculations.

2.1 Radiation

2.1.1 Top-of-the-atmosphere solar radiation

The calculation of C_n and E_n^a begin with modeling the extraterrestrial solar radiation flux, I_o ($\mathrm{W\,m^{-2}}$). The equation for I_o may be expressed as the product of three terms (Duffie and Beckman, 2013):

$$I_o = I_{sc}\, d_r\, \cos\theta_z, \tag{2}$$

where I_{sc} ($\mathrm{W\,m^{-2}}$) is the solar constant, d_r (unitless) is the distance factor, and $\cos\theta_z$ (unitless) is the inclination factor. Values for I_{sc} may be found in the literature (e.g., Thekaekara and Drummond, 1971; Willson, 1997; Dewitte et al., 2004; Fröhlich, 2006; Kopp and Lean, 2011); a constant for I_{sc} is given in Table 2.

The distance factor, d_r, accounts for additional variability in I_o that reaches the Earth. This variability is due to the relative change in distance between Earth and the Sun caused by the eccentricity of Earth's elliptical orbit, e (unitless), and is calculated as (Berger et al., 1993):

$$d_r = \left(\frac{1 + e\,\cos\nu}{1 - e^2}\right)^2, \tag{3}$$

where ν (rad) is Earth's true anomaly. True anomaly is the measure of Earth's location around the Sun relative to its position when it is closest to the Sun (perihelion).

The last term, $\cos\theta_z$, attenuates I_o to account for the Sun's height above the horizon (measured relative to the zenith angle, θ_z), accounting for the off-vertical tilt of Earth's rotational axis, ε (i.e., obliquity). The inclination factor is calculated as (Duffie and Beckman, 2013):

$$\cos\theta_z = \sin\delta\,\sin\phi + \cos\delta\,\cos\phi\,\cos h, \tag{4}$$

where ϕ (rad) is the latitude, δ (rad) is the declination angle, and h (rad) is the hour angle, measuring the angular displacement of the Sun east or west of solar noon ($-\pi \le h \le \pi$). Declination is the angle between Earth's equator and the Sun at solar noon ($h = 0$), varying from $+\varepsilon$ at the June solstice to $-\varepsilon$ at the December solstice; the changing declination is responsible for the change in seasons. For the purposes of ecological modeling, δ may be assumed constant throughout a single day. See e.g. Woolf (1968) for the precise geometric equation representing δ:

$$\delta = \arcsin\left(\sin\lambda\,\sin\varepsilon\right), \tag{5}$$

where λ (rad) is Earth's true longitude (i.e., the heliocentric longitude relative to Earth's position at the vernal equinox) and ε (rad) is obliquity (i.e., the slowly varying tilt of Earth's axis). Several other methods are widely used for the estimation of δ for a given day of the year (e.g., Cooper, 1969; Spencer, 1971; Swift, 1976) but are not recommended because they do not

Geosci. Model Dev. Discuss., doi:10.5194/gmd-2016-49, 2016
Manuscript under review for journal Geosci. Model Dev.
Published: 15 April 2016

Geoscientific Model Development Discussions

account for the change in Earth's orbital velocity with respect to the distance between Earth and the Sun, while Eq. 5 does. The relationship between true longitude, λ, and true anomaly, ν, is by the angle of the perihelion with respect to the vernal equinox, $\widetilde{\omega}$ (rad) (Berger, 1978):

$$\nu = \lambda - \widetilde{\omega}. \tag{6}$$

While the three orbital parameters (i.e., e, ε, and $\widetilde{\omega}$) exhibit long-term variability (on the order of tens of thousands of years), they may be treated as constants for a given epoch (e.g., $e = 0.0167$, $\varepsilon = 23.44°$, and $\widetilde{\omega} = 283.0°$ for 2000 CE), which can be calculated using the methods of Berger (1978) or Berger and Loutre (1991). Berger (1978) presents a simple algorithm to estimate λ for a given day of the year (see Appendix A).

The daily top-of-the-atmosphere solar radiation, H_o (J m^{-2}), may be calculated as twice the integral of I_o measured between solar noon and the sunset angle, h_s, assuming that all angles related to Earth on its orbit are constant over a whole day:

$$H_o = \int_{day} I_o = 2 \int_{h=0}^{h_s} I_o = \frac{86\,400}{\pi} I_{sc}\, d_r\, (h_s \sin\delta \sin\phi + \cos\delta \cos\phi \sin h_s). \tag{7}$$

The sunset angle can be calculated as the hour angle when the solar radiation flux reaches the horizon (i.e., when $I_o = 0$) and can found by substituting Eq. 4 into Eq. 2, setting I_o equal to zero, and solving for h:

$$h_s = \arccos\left(-\frac{r_u}{r_v}\right), \tag{8}$$

where $r_u = (\sin\delta \sin\phi)$ and $r_v = (\cos\delta \cos\phi)$, both unitless. To account for the occurrences of polar day (i.e., no sunset) and polar night (i.e., no sunrise), h_s should be limited to π when $r_u/r_v \geq 1$ and zero when $r_u/r_v \leq -1$.

2.1.2 Net surface radiation

The daytime (positive) net surface radiation, H_N (J m^{-2}), is the integral of the net surface radiation flux received at the land surface, I_N (W m^{-2}), which is classically defined as the difference between the net incoming shortwave radiation flux, I_{SW} (W m^{-2}) and the net outgoing longwave radiation flux, I_{LW} (W m^{-2}):

$$I_N = I_{SW} - I_{LW}. \tag{9}$$

The calculation of I_{SW} is based on the reduction in I_o due to atmospheric transmittivity, τ (unitless), and surface shortwave albedo, β_{sw} (unitless):

$$I_{SW} = (1 - \beta_{sw})\, \tau\, I_o. \tag{10}$$

A constant value for β_{sw} is given in Table 2. Atmospheric transmittivity may be expressed as a function of elevation (to account for attenuation caused by the mass of the atmosphere) and cloudiness (to account for atmospheric turbidity). At higher elevations, there is less atmosphere through which shortwave radiation must travel before reaching the surface. To account

Geosci. Model Dev. Discuss., doi:10.5194/gmd-2016-49, 2016
Manuscript under review for journal Geosci. Model Dev.
Published: 15 April 2016

Geoscientific Model Development Discussions
Open Access
EGU

for this, Allen (1996) presents an equation based on the regression of Beer's radiation extinction function at elevations below 3000 m with an average sun angle of 45°, which can be expressed as:

$$\tau = \tau_o \left(1 + 2.67 \times 10^{-5}\, z\right), \tag{11}$$

where z (m) is the elevation above mean sea level and τ_o (unitless) is the mean sea-level transmittivity, which can be approximated by the Ångstrom-Prescott formula:

$$\tau_o = c + d\, S_f, \tag{12}$$

where c and d are empirical constants (unitless) and S_f is the fraction of daily bright sunshine hours ($0 \leq S_f \leq 1$). Values for c and d are given in Table 2.

The calculation of I_{LW} is based on the difference between outgoing and incoming longwave radiation fluxes attenuated by the presence of clouds, which may be empirically estimated by (Linacre, 1968):

$$I_{LW} = [b + (1 - b)\ S_f]\,(A - T_{air}), \tag{13}$$

where A and b are empirical constants and T_{air} (°C) is the mean air temperature. The outgoing longwave radiation flux used to derive Eq. 13 assumes a constant ground emissivity, which is accurate under well-watered conditions. The incoming longwave radiation flux is modeled based on clear-sky formulae derived by Linacre (1968). Values for A and b are given in Table 2.

H_N, similarly to H_o, may be calculated as twice the integral of I_N between solar noon and the net surface radiation flux cross-over hour angle, h_n (rad):

$$H_N = \int_{day} I_N = 2 \int_{h=0}^{h_n} I_N = \frac{86\,400}{\pi}\ [(r_w\, r_u - I_{LW})\ h_n + r_w\, r_v\ \sin h_n], \tag{14}$$

where $r_w = (1 - \beta_{sw})\, \tau\, I_{sc}\, d_r$ (W m^{-2}).

Here h_n is the hour angle when I_{SW} equals I_{LW} (i.e., when I_N = 0) and, following the substitution of Eq. 10 and Eq. 13 for I_{SW} and I_{LW}, respectively, may be expressed as:

$$h_n = \arccos\left(\frac{I_{LW} - r_w\, r_u}{r_w\, r_v}\right). \tag{15}$$

To account for the occurrences when the net surface radiation flux does not cross the zero datum, h_n should be limited to π when $(I_{LW} - r_w\, r_u)/(r_w\, r_v) \leq -1$ (i.e., net surface radiation flux is always positive) and zero when $(I_{LW} - r_w\, r_u)/(r_w\, r_v) \geq 1$ (i.e., net surface radiation flux is always negative).

The night-time (negative) net surface radiation, H_N^* (J m^{-2}), consists of two parts: I_N for $h_n \leq h \leq hs$ and I_{LW} for $h_s \leq h \leq \pi$. The calculation consists of doubling the half-day integrals:

$$H_N^* = 2 \int_{h_n}^{\pi} I_N = 2 \left(\int_{h_n}^{h_s} I_N + \int_{h_s}^{\pi} I_{LW} \right), \tag{16a}$$

Geosci. Model Dev. Discuss., doi:10.5194/gmd-2016-49, 2016
Manuscript under review for journal Geosci. Model Dev.
Published: 15 April 2016

Geoscientific Model Development Discussions

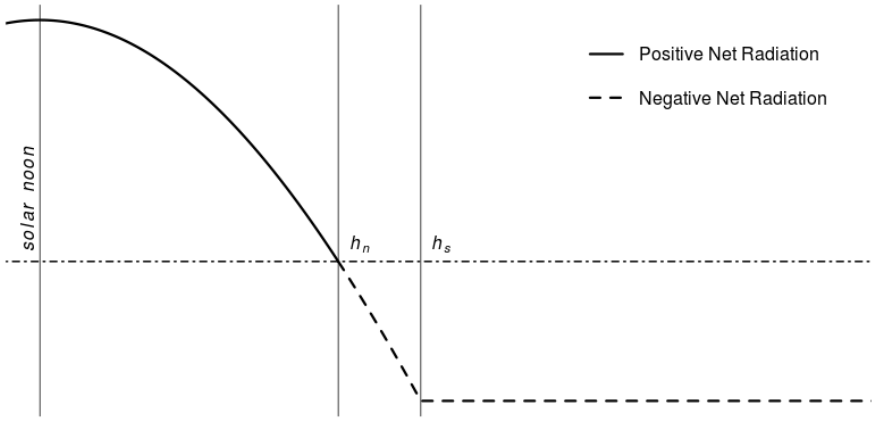

Figure 1. Example of a half-day net radiation flux curve with time represented along the x-axis. Positive values of I_N, shown decreasing from solar noon to zero at the cross-over hour angle, h_n, is denoted with a bold solid line, while negative values of I_N, which continues to decrease from h_n to a minimum at the sunset hour angle, h_s, is denoted with a bold dashed line. The dash-dotted line marks the datum of zero radiation.

which may be expressed as (note that H_N^* is a negative quantity):

$$H_N^* = \frac{86\,400}{\pi}\left[r_w\, r_u\,(h_s - h_n) + r_w\, r_v\,(\sin h_s - \sin h_n) + I_{LW}\,(\pi - 2\,h_s + h_n)\right]. \tag{16b}$$

Figure 1 shows an example of a half-day I_N curve used in the integrals defined in Eqns. 14 and 16. I_N, which is at its peak at solar noon, crosses zero at h_n and reaches a minimum at h_s. After sunset (i.e., $h > h_s$), when I_{SW} is zero, I_N is equal to $-I_{LW}$. H_N is represented as twice the integral under the positive net radiation curve (solid line), above the zero line (dash-dotted line), and between the vertical lines of solar noon and h_n. H_N^* is represented as twice the integral below the zero line and above the negative net radiation curve (the two dashed lines).

2.1.3 Photosynthetically active radiation

The daily photosynthetically active radiation in units of photon flux density, Q_n ($\mathrm{mol\,m^{-2}\,d^{-1}}$), is calculated based on the number of quanta received (moles of photons) within the visible light spectrum, which also corresponds to the action spectrum of photosynthesis (Monteith and Unsworth, 1990):

$$Q_n = 1 \times 10^{-6}\ \mathrm{fFEC}\ (1 - \beta_{vis})\ \tau\ H_o, \tag{17}$$

where β_{vis} (unitless) is the visible light albedo and fFEC ($\mu\mathrm{mol\,J^{-1}}$) is the flux-to-energy conversion factor (Ge et al., 2011). This factor takes into account both the portion of visible light within the total solar spectrum, approximately 50% (Stanhill and Fuchs, 1977), and the mean number of quanta in the visible light energy band, approximately 4.6 $\mu\mathrm{mol\,J^{-1}}$ (McCree, 1972). The 1×10^{-6} converts the units of Q_n from $\mu\mathrm{mol\,m^{-2}\,d^{-1}}$ to $\mathrm{mol\,m^{-2}\,d^{-1}}$. Values for β_{vis} and fFEC are given in Table 2.

Geosci. Model Dev. Discuss., doi:10.5194/gmd-2016-49, 2016
Manuscript under review for journal Geosci. Model Dev.
Published: 15 April 2016

Geoscientific Model Development Discussions
Open Access
EGU

2.2 Condensation

The daily condensation, C_n, may be expressed as the water-equivalent of the absolute value of negative net radiation, H_N^*:

$$C_n = 1 \times 10^3 \, E_{con} \, |H_N^*|, \tag{18}$$

where E_{con} ($\mathrm{m^3\,J^{-1}}$) is the water-to-energy conversion factor that relates the energy released or required for a unit volume of water to evaporate or condense at a given temperature and pressure, which may be expressed as:

$$E_{con} = \frac{s}{L_v \, \rho_w \, (s+\gamma)}, \tag{19}$$

where s ($\mathrm{Pa\,K^{-1}}$) is the slope of the saturation vapor pressure-temperature curve, L_v ($\mathrm{J\,kg^{-1}}$) is the latent heat of vaporization of water, ρ_w ($\mathrm{kg\,m^{-3}}$) is the density of water, and γ ($\mathrm{Pa\,K^{-1}}$) is the psychrometric constant. Standard values may be assumed for certain parameters (e.g., $L_v = 2.5 \times 10^6$ $\mathrm{J\,kg^{-1}}$; $\rho_w = 1 \times 10^3$ $\mathrm{kg\,m^{-3}}$; $\gamma = 65$ $\mathrm{Pa\,K^{-1}}$); however, equations for the temperature dependence of s and L_v (e.g., Allen et al., 1998; Henderson-Sellers, 1984) and the temperature and pressure dependence of ρ_w and γ (e.g., Kell, 1975; Chen et al., 1977; Allen et al., 1998; Tsilingiris, 2008) are available (see Appendix B).

The barometric formula may be used to estimate the atmospheric pressure, P_{atm} (Pa), at a given elevation, z (m), when observations are not available. Assuming a linear decrease in temperature with height, which is a reasonable approximation within the troposphere (i.e., for $z < 1.10 \times 10^4$ m), the following equation may be used (Berberan-Santos et al., 1997):

$$P_{atm} = P_o \left(1 - \frac{L\,z}{T_o}\right)^{\frac{g\,M_a}{R\,L}}, \tag{20}$$

where P_o (Pa) is the base pressure, T_o (K) is the base temperature, z (m) is the elevation above mean sea level, L ($\mathrm{K\,m^{-1}}$) is the mean adiabatic lapse rate of the troposphere, g ($\mathrm{m\,s^{-2}}$) is the standard gravity, M_a ($\mathrm{kg\,mol^{-1}}$) is the molecular weight of dry air, and R ($\mathrm{J\,mol^{-1}\,K^{-1}}$) is the universal gas constant. Values for the constants used in Eq. 20 are given in Table 2.

2.3 Evaporative Supply

The evaporative supply rate, S_w ($\mathrm{mm\,h^{-1}}$) is assumed to be constant over the day and can be estimated based on a linear proportion of the previous day's soil moisture, W_{n-1} (Federer, 1982):

$$S_w = S_c \, \frac{W_{n-1}}{W_m}, \tag{21}$$

where S_c ($\mathrm{mm\,h^{-1}}$) is the supply rate constant (i.e., maximum rate of evaporation) and W_m (mm) is the maximum soil moisture capacity. Constant values for S_c and W_m are given in Table 2. Although in principle W_m could be formulated as a property of soil type (as was done, for example, in the original BIOME model), there are several objections to doing so. One is that the seasonal course of soil moisture in the 'bucket model' formulation is insensitive to the exact value specified for W_m. Another is that although W_m has a standard definition (as the difference between field capacity and wilting point) in agronomy, the wilting point in reality depends on plant properties. Yet another is that the effective 'bucket size' depends on rooting behavior, which is highly adaptable to the soil wetness profile. Thus, we suggest that no meaningful improvement in realism is likely to be achieved by applying soil type-dependent values of W_m.

Geosci. Model Dev. Discuss., doi:10.5194/gmd-2016-49, 2016
Manuscript under review for journal Geosci. Model Dev.
Published: 15 April 2016

Geoscientific Model Development Discussions
Open Access
EGU

2.4 Evaporative Demand

The evaporative demand rate, D_p ($\mathrm{mm\,h^{-1}}$), is set equal to the potential evapotranspiration rate, E^p ($\mathrm{mm\,h^{-1}}$), as defined by Priestley and Taylor (1972). E^p usually exceeds the equilibrium evapotranspiration rate, E^q ($\mathrm{mm\,h^{-1}}$), due to the entrainment of dry air in the convective boundary layer above an evaporating surface (Raupach, 2000, 2001). E^p is related to E^q by the Priestley-Taylor coefficient, which may be defined as one plus an entrainment factor, ω (Lhomme, 1997):

$$D_p = E^p = (1+\omega)\ E^q. \tag{22}$$

The constant value used for ω is given in Table 2. The calculation of E^q is based on the energy-water equivalence of I_N, ignoring the soil heat flux, (Lhomme, 1997):

$$E^q = 3.6 \times 10^6\ E_{con}\ I_N, \tag{23}$$

where 3.6×10^6 converts the units of E^q from $\mathrm{m\,s^{-1}}$ to $\mathrm{mm\,h^{-1}}$. Note that E^q is defined only for positive values (i.e., $E^q = 0$ for $I_N < 0$). The Priestley-Taylor potential evapotranspiration is preferred in this context to the general Penman-Monteith equation for actual evapotranspiration (Penman, 1948; Monteith, 1965), which requires knowledge of stomatal and aerodynamic conductances, or to any of the 'reference evapotranspiration' formulae (Allen et al., 1998) that specifically relate to agricultural crops.

Daily equilibrium evapotranspiration, E^q_n ($\mathrm{mm\,d^{-1}}$), is based on the integration of Eq. 23, or simply the energy-water equivalence of H_N:

$$E^q_n = 1 \times 10^3\ E_{con}\ H_N, \tag{24}$$

where 1×10^3 converts E^q_n from $\mathrm{m\,d^{-1}}$ to $\mathrm{mm\,d^{-1}}$.

The daily demand, which is equal to the daily potential evapotranspiration, E^p_n ($\mathrm{mm\,d^{-1}}$), may be calculated from E^q_n, as in Eq. 22:

$$E^p_n = (1+\omega)\ E^q_n. \tag{25}$$

2.5 Actual Evapotranspiration

The calculation of daily actual evapotranspiration, E^a_n ($\mathrm{mm\,d^{-1}}$), is based on the daily integration of the actual evapotranspiration rate, E^a ($\mathrm{mm\,h^{-1}}$), which may be defined as the minimum of the evaporative supply and demand rates (Federer, 1982):

$$E^a = \min\left(S_w, D_p\right), \tag{26}$$

where S_w ($\mathrm{mm\,h^{-1}}$) is the evaporative supply rate, defined in Eq. 21, and D_p ($\mathrm{mm\,h^{-1}}$) is the evaporative demand rate, defined in Eq. 22.

Geosci. Model Dev. Discuss., doi:10.5194/gmd-2016-49, 2016
Manuscript under review for journal Geosci. Model Dev.
Published: 15 April 2016

Geoscientific Model Development Discussions

The analytical solution to E_n^a may be expressed analogous to the methodology used for solving H_o and H_N and is defined as twice the integral of E^a between solar noon and h_n, which comprises two curves: S_w for $0 \le h \le h_i$ and D_p for $h_i \le h \le h_n$, where h_i (rad) is the hour angle corresponding to the intersection of S_w and D_p (i.e., when $S_w = D_p$):

$$E_n^a = 2 \int_{h=0}^{h_n} E^a = 2 \left(\int_0^{h_i} S_w + \int_{h_i}^{h_n} D_p \right), \tag{27a}$$

which may be expressed as:

$$E_n^a = \frac{24}{\pi} \left[S_w \, h_i + r_x \, r_w \, r_v \, (\sin h_n - \sin h_i) + (r_x \, r_w \, r_u - r_x \, I_{LW}) \, (h_n - h_i) \right], \tag{27b}$$

where $r_x = 3.6 \times 10^6 \, (1 + \omega) \, E_{con}$ ($\mathrm{mm\,m^2\,W^{-1}\,h^{-1}}$). The intersection hour angle, h_i, is defined by setting Eq. 21 equal to Eq. 22 and solving for h:

$$h_i = \arccos \left(\frac{S_w}{r_x \, r_w \, r_v} + \frac{I_{LW}}{r_w \, r_v} - \frac{r_u}{r_v} \right). \tag{28}$$

To account for the occurrences when supply is in excess of demand during the entire day, h_i should be limited to zero when $\cos h_i \ge 1$. For occurrences when supply limits demand during the entire day, h_i should be limited to π when $\cos h_i \le -1$.

Figure 2 shows an example of the half-day evaporative supply and demand rate curves. D_p (dashed line) is at a maximum at solar noon and decreases down to zero at h_n, while S_w (dotted line) is constant throughout the day. The point where S_w equals D_p is denoted by the vertical bar at h_i. E^a (bold solid line), limited by supply during most of the day, follows the S_w line between solar noon and h_i. During the time between h_i and h_n, E^a no longer limited by supply, follows the D_p curve. After h_n, both D_p and E^a are zero. E_n^a is represented by twice the area above the zero line (dash-dotted line), below the bold solid lines of E^a, and between the vertical bars of solar noon and h_n.

2.6 Soil Moisture

With analytical expressions for C_n and E_n^a (i.e., Eqns. 18 and 27b, respectively), W_n may be calculated by Eq. 1. Daily soil moisture in excess of the maximum soil moisture capacity, W_m, is assumed to be runoff, RO (mm), and may be calculated as:

$$RO = \max(0, W_n - W_m). \tag{29}$$

To account for the occurrences when W_n exceeds W_m or when W_n drops below zero, the following limits have to be applied to W_n following the calculation of RO:

$$W_n = \begin{cases} W_m, & \text{if } W_n \ge W_m \\ 0, & \text{if } W_n \le 0. \end{cases} \tag{30}$$

The limiting effect of S_w on E_n^a, through Eqns. 27 and 28, should, in most cases, prevent W_n from falling below zero; however, due to the assumption that S_w is constant throughout the day, there is the possibility that E_n^a may exceed $W_{n-1} + P_n + C_n$, resulting in negative W_n. In these rare cases, in order to maintain the mass balance of the bucket model presented in Eq. 1, E_n^a is reduced by an amount equal to the magnitude of the negative soil moisture.

Geosci. Model Dev. Discuss., doi:10.5194/gmd-2016-49, 2016
Manuscript under review for journal Geosci. Model Dev.
Published: 15 April 2016

Geoscientific Model Development Discussions

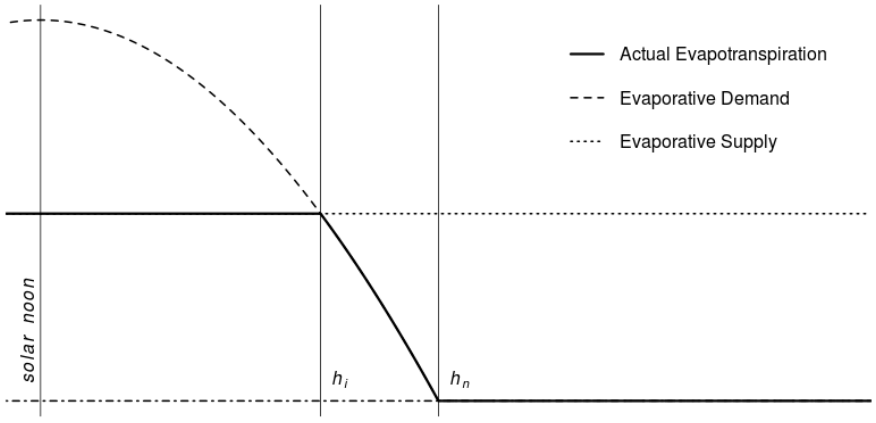

Figure 2. Example of half-day evaporative supply and demand curves with time represented along the x-axis. Evaporative demand, D_p (dashed line), is at a maximum at solar noon and zero at the cross-over hour angle, h_n. The evaporative supply, S_w (dotted line), is constant throughout the day. The point where supply is equal to demand denotes the intersection hour angle, h_i. Actual evapotranspiration (bold line) is defined as the minimum of S_w and D_p throughout the day.

3 Bioclimatic Indices

One application of the SPLASH model is estimating the surface fluxes required for the calculation of bioclimatic indices. Typically described at longer time scales (e.g., monthly or annually), the daily SPLASH fluxes can be aggregated to monthly and annual totals:

$$X_{m,a} = \sum_{d=1}^{N_{m,a}} X_d, \tag{31}$$

where X is a model output parameter at a given day (X_d), month (X_m), or year (X_a) and N is the total number of days to sum over for a given month (N_m) or a given year (N_a).

The following sections describe three common bioclimatic indices.

3.1 Moisture Index

There exists a long history that includes several variants of the moisture index, MI, also commonly referred to as the aridity index, AI, or moisture ratio, MR (Thornthwaite, 1948; Budyko, 1961). A current definition describes MI as the ratio of annual precipitation to annual potential evapotranspiration (Middleton and Thomas, 1997), given as:

$$MI = \frac{P_a}{E_a^p}, \tag{32}$$

where P_a ($\mathrm{mm\,a^{-1}}$) is the annual precipitation and E_a^p ($\mathrm{mm\,a^{-1}}$) is the annual potential evapotranspiration as calculated by Eq. 31; P_a and E_a^p may be substituted with their multi-year means (i.e., $\bar{P}_a$ and $\bar{E}_a^p$) if available. Values less than one are indicative of annual moisture deficit.

Geosci. Model Dev. Discuss., doi:10.5194/gmd-2016-49, 2016
Manuscript under review for journal Geosci. Model Dev.
Published: 15 April 2016

Geoscientific Model Development Discussions
Open Access
EGU

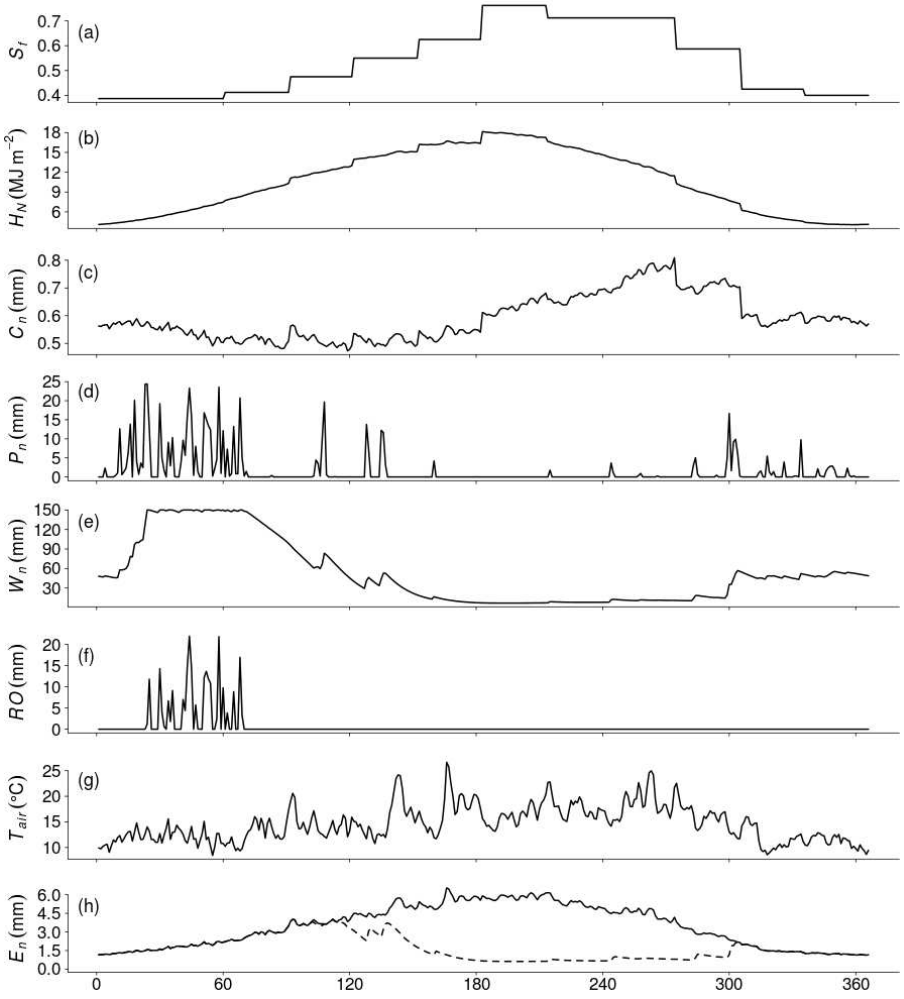

Figure 3. Model results and input data of daily (a) fraction of bright sunshine hours, S_f (CRU TS); (b) positive net surface radiation, H_N; (c) condensation, C_n; (d) precipitation, P_n (WATCH); (e) soil moisture, W_n; (f) runoff, RO; (g) mean air temperature, T_{air} (WATCH); and (h) potential (solid line) and actual (dashed) evapotranspiration, E_n^p and E_n^a, respectively. Days of the year are represented along the x-axis. Data are for one year (2000 CE) in San Francisco, United States.

3.2 Climatic Water Deficit

The climatic water deficit, ΔE, defined as the difference between the evaporative demand (i.e., potential evapotranspiration) and the actual evapotranspiration, has been shown to be a biologically meaningful measure of climate as it pertains to both the magnitude and length of drought stress experienced by plants (Stephenson, 1998). At the monthly timescale, this index is calculated as:

$$\Delta E_m = E_m^p - E_m^a, \tag{33}$$

Geosci. Model Dev. Discuss., doi:10.5194/gmd-2016-49, 2016
Manuscript under review for journal Geosci. Model Dev.
Published: 15 April 2016

Geoscientific Model Development Discussions

where ΔE_m ($\mathrm{mm\,mo^{-1}}$) is the monthly climatic water deficit, E_m^p ($\mathrm{mm\,mo^{-1}}$) is the monthly potential evapotranspiration and E_m^a ($\mathrm{mm\,mo^{-1}}$) is the monthly actual evapotranspiration. E_m^p and E_m^a are the monthly totals of E_n^p and E_n^a, respectively, calculated by Eq. 31. Values of ΔE may also be computed at the annual timescale.

3.3 Priestley-Taylor Coefficient

The Priestley-Taylor coefficient, α, is the ratio of actual evapotranspiration to equilibrium evapotranspiration, which represents the fraction of plant-available surface moisture (Priestley and Taylor, 1972; Sykes et al., 1996; Gallego-Sala et al., 2010). At the monthly timescale, this is defined as:

$$\alpha_m = \frac{E_m^a}{E_m^q}, \tag{34}$$

where α_m is the monthly Priestley-Taylor coefficient, E_m^a is the monthly actual evapotranspiration and E_m^q ($\mathrm{mm\,mo^{-1}}$) is the monthly equilibrium evapotranspiration. Values of α may also be computed at the annual timescale.

4 Results

The methodology described in Sect. 2 was translated into computer application code (C++, FORTRAN, Python and R). Data were assembled for one year (2000 CE) including daily WATCH precipitation and air temperature and monthly CRU TS3.21 cloudiness fraction. At each time step, data were extracted from a single $0.5^\circ \times 0.5^\circ$ pixel above San Francisco, United States (i.e., 37.75° N, 122.25° W). The mean daily air temperature was converted from K to $^\circ$C and the mean daily precipitation was converted from $\mathrm{kg\,m^{-2}\,s^{-1}}$ to $\mathrm{mm\,d^{-1}}$ assuming a constant density of water (i.e., $\rho_w = 1 \times 10^3\ \mathrm{kg\,m^{-3}}$). Fractional sunshine hours were assumed equal to the one-complement of cloudiness fraction and were assumed constant over each month. Figures 3a, 3d, and 3g show the experimental data for S_f, P_n, and T_{air}, respectively.

Approximate values were given for the latitude, 37.7° (0.658 rad), and elevation above mean sea level, 142 m, and model constants were assigned as per Table 2. The daily soil moisture was initialized at zero and allowed to stabilize, which occurred after just two year-long model iterations. After the second iteration, the daily and monthly results showed no appreciable change and are presented in Figs. 3 and 4.

Figure 3b shows the H_N curve ($\mathrm{MJ\,m^{-2}}$), which has the characteristic bell-shaped curve of radiation in the northern hemisphere. The slight jumps between months are due to the irregular jumps in the S_f data (i.e., Fig. 3a). Figure 3c shows the results for C_n, which based on Eq. 18 is a function of H_N^* and also displays the monthly jumps due to S_f. Additional fluctuations in C_n due to the air temperature (i.e., Fig. 3g) can also be seen as influenced by the temperature dependency of E_{con}. The magnitude of C_n varies over the year between 0.45 and 0.8 mm, which is small when compared to the magnitude of daily rainfall occurrences during the winter months that, in some instances, exceeds 20 $\mathrm{mm\,d^{-1}}$ as shown in Fig. 3d.

Daily soil moisture, W_n, is shown in Fig. 3e. The heavy rains at the beginning of the year (as shown in Fig. 3d) produced saturated soil conditions (i.e., $W_n = W_m = 150$ mm), which gradually reduced as the rainy season came to an end. Small spikes in the soil moisture are seen during the infrequent rain events throughout the spring and summer when soil moisture was

Geosci. Model Dev. Discuss., doi:10.5194/gmd-2016-49, 2016
Manuscript under review for journal Geosci. Model Dev.
Published: 15 April 2016

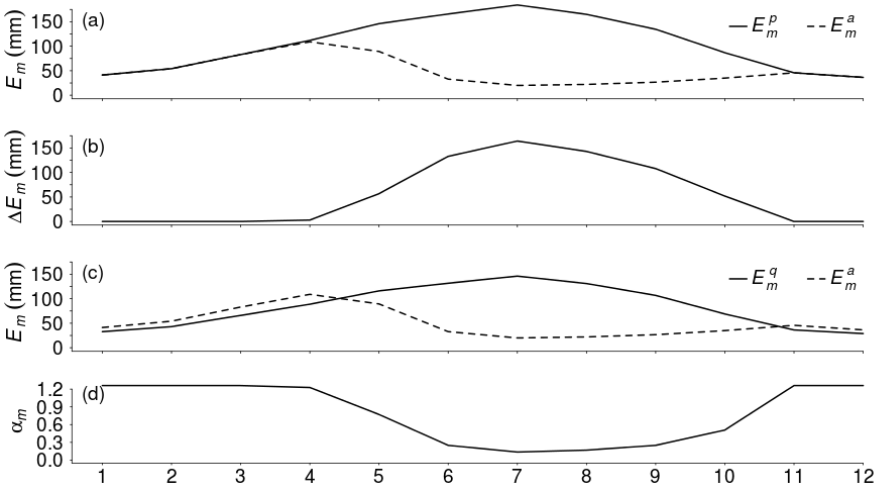

Figure 4. Model results of monthly (a) potential (solid line) and actual (dashed line) evapotranspiration, E_m^p and E_m^a, respectively; (b) climatic water deficit, ΔE_m; (c) equilibrium (solid) and actual (dashed line) evapotranspiration, E_m^q and E_m^a, respectively; and (d) monthly Priestley-Taylor coefficient, α_m. Months of the year are represented along the x-axis. Results are of one year (2000 CE) for San Francisco, United States.

maintained at a low level (< 10 mm). At the end of October, when the rains began again, soil moisture began to be replenished. While W_n was saturated, runoff was produced due to the excess in rainfall (shown in Fig. 3f).

Figure 3h shows the overlay of E_n^p (solid line) and E_n^a (dashed line). During the winter and early spring when D_p was relatively low and S_w was non-limiting due to the high soil moisture conditions, E_n^a is shown following the E_n^p curve. As D_p continued to increase into the summer, E_n^a fell below the E_n^p curve due to the depletion of soil moisture. The small spikes in soil moisture from rainfall events throughout the late spring and summer can be seen translated into the E_n^a curve. When the rains began again in the autumn replenishing soil moisture and D_p had decreased due to the seasonal change in radiation, E_n^a is once again shown following the E_n^p curve.

The same trend shown in Fig. 3h can be seen at the monthly time scale in Fig. 4a, where E_m^a (dashed line) is shown following E_m^p (solid line) during the first three months, then drops below for the following seven months, and for the last month, once again is following the E_m^p curve. The difference between E_m^p and E_m^a is the climatic water deficit (i.e., Eq. 33), which is shown in Fig. 4b, which highlights the months when supply was limited.

Figure 4c shows the comparison between E_m^q (i.e., E_m^p with zero entrainment) and E_m^a. The ratio of E_m^a to E_m^q is the Priestley-Taylor coefficient, α_m (i.e., Eq. 34). Due to the entrainment factor, α_m may vary between zero (i.e., no moisture) and $1 + \omega$ (i.e., unlimited moisture). During the months when supply is not limiting and ΔE_m is zero, α_m is at a maximum, as shown in Fig. 4d. Similarly, for months when supply is limiting and ΔE_m is positive, a reduction in α_m occurs.

At the annual timescale, ΔE_a is 660 mm, which is greater than the annual precipitation (i.e., 620 mm). The annual moisture index (i.e., $MI = 0.493$) and Priestley-Taylor coefficient (i.e., $\alpha_a = 0.598$) are both less than one. These three bioclimatic

Geosci. Model Dev. Discuss., doi:10.5194/gmd-2016-49, 2016
Manuscript under review for journal Geosci. Model Dev.
Published: 15 April 2016

Geoscientific Model Development Discussions

indices concur that the year was water stressed, which is unsurprising given the frequent occurrence of summer droughts in the western United States.

5 Discussion

The results presented in Sect. 4 are intended to illustrate the dynamic changes in each variable from wet to dry seasons for a steady-state system. It should be noted that this work intends only to facilitate the development and application of this model and does not purport to be an in-depth analysis of processes.

While the methodology presented in Sect. 2 makes numerous assumptions and simplifications (e.g., invariant soil properties; physically predictable vegetation function; no infiltration-excess runoff), it provides a simple and robust framework for the estimation of radiation components, evapotranspiration, and plant-available moisture requiring only standard meteorological measurements as input. Under steady-state conditions, the SPLASH model preserves the water balance, such that:

$$\sum (P_n + C_n) = \sum (E_n^a + RO)\,. \tag{35}$$

Over the years, a common misconception has developed regarding the calculation of daily actual evapotranspiration (as defined by Federer, 1982), whereby the integration of Eq. 26 is mistakenly interpreted as:

$$E_n^a = \min(S, D)\,, \tag{36}$$

where D ($\mathrm{mm\,d^{-1}}$) is the total daily demand, given by Eq. 25, and S ($\mathrm{mm\,d^{-1}}$) is the total daily supply over the hours of positive net radiation, which may be given by:

$$S = \int_{day} S_w = \int_{-h_n}^{h_n} S_w = \frac{24}{\pi}\, h_n\, S_w, \tag{37}$$

where h_n is the net radiation cross-over angle, given by Eq. 15, and the constant coefficient converts the units of radians to hours. As shown in Fig. 2, E_n^a is a piecewise function consisting of two curves overlaid throughout the course of a single day that must be accounted for simultaneously; however, even in some recent model developments, E_n^a is calculated using Eq. 36, including the equilibrium terrestrial biosphere models BIOME3 and BIOME4 (Haxeltine and Prentice, 1996; Kaplan, 2001) and the Lund-Potsdam-Jena Dynamic Global Vegetation Model (Sitch et al., 2003). Only under specific circumstances will Eq. 36 produce correct results. It is the intension of this work to provide a simple analytical solution that correctly accounts for the integration of Eq. 26, which has been provided in the form of Eq. 27b.

Code Availability

The code, in four programming languages (C++, FORTRAN, Python, and R), is available on an online repository under the GNU Lesser General Public License (https://bitbucket.org/labprentice/splash). The repository includes the present release

Geosci. Model Dev. Discuss., doi:10.5194/gmd-2016-49, 2016
Manuscript under review for journal Geosci. Model Dev.
Published: 15 April 2016

Geoscientific Model Development Discussions
Open Access
EGU

(v1.0) and working development of the code (with Makefiles where appropriate), example data, and the user manual. All four versions of the code underwent and passed a set of consistency checks to ensure similar results were produced under the same input conditions. The following describes the requirements for compiling and executing SPLASH v.1.0.

For the C++ version, the code was successfully compiled and executed using the GNU C++ compiler (g++ v.4.8.2) provided by the GNU Compiler Collection (Free Software Foundation, Inc., 2016). It utilizes the C numerics library (cmath), input/output operations library (cstdio), and the standard general utilities library (cstdlib) and references the vector container and string type.

For the FORTRAN version, the code was successfully compiled and executed using the PGI Fortran compiler (pgf95 v.16.1-0) provided by The Portland Group - PGI Compilers and Groups (NVIDIA Corporation, 2016) and the GNU Fortran compiler (gfortran v.4.8.4) provided by the GNU Compiler Collection (Free Software Foundation, Inc., 2016).

For the Python version, the code was successfully compiled and executed using Python 2.7 and Python 3.5 interpreters (Python Software Foundation, 2016). It requires the installation of third-party packages, including NumPy (v.1.10.4 by NumPy Developers, 2016) and SciPy (v.0.17.0 by SciPy Developers, 2016) and utilizes the basic date and time types (datetime), logging facility (logging), Unix-style pathname pattern extension (glob), and miscellaneous operating system interfaces (os) modules.

For the R version, the code was successfully compiled and executed using R-3.2.3 "Wooden Christmas-Tree" (The R Foundation for Statistical Computing, 2015).

Appendix A: Calculating True Longitude

Berger (1978) presents a method for estimating true longitude, λ, for a given day of the year, n, that associates uniform time (i.e., a mean planetary orbit and constant day of the vernal equinox) to Earth's angular position. The formula is based on classical astronomy and is suitable for calculations in palaeoclimatology. The algorithm begins with the calculation of the mean longitude of the vernal equinox, λ_{m0} (rad), assumed to fall on 21 March:

$$\lambda_{m0} = 2\left[\left(\frac{1}{2}\,e + \frac{1}{8}\,e^3\right)(1+\beta)\,\sin\widetilde{\omega} - \frac{1}{4}\,e^2\left(\frac{1}{2}+\beta\right)\sin 2\widetilde{\omega} + \frac{1}{8}\,e^3\left(\frac{1}{3}+\beta\right)\sin 3\widetilde{\omega}\right], \tag{A1}$$

where $\beta = \sqrt{1-e^2}$. The mean longitude, λ_m (rad), is then calculated for a given day based on a daily increment with respect to the day of the vernal equinox (i.e., day 80):

$$\lambda_m = \lambda_{m0} + 2\pi\,(n-80)\,N_a^{-1}, \tag{A2}$$

where N_a is total number of days in the year. The mean anomaly, ν_m (rad), is calculated based on the equality presented in Eq. 6:

$$\nu_m = \lambda_m - \widetilde{\omega}, \tag{A3}$$

which is then used to determine the true anomaly by:

$$\nu = \nu_m + \left(2e - \frac{1}{4}\,e^3\right)\sin\nu_m + \frac{5}{4}\,e^2\,\sin 2\nu_m + \frac{13}{12}\,e^3\,\sin 3\nu_m, \tag{A4}$$

Geosci. Model Dev. Discuss., doi:10.5194/gmd-2016-49, 2016
Manuscript under review for journal Geosci. Model Dev.
Published: 15 April 2016

Geoscientific Model Development Discussions
Open Access
EGU

and is converted back to true longitude by:

$$\lambda = \nu + \widetilde{\omega}. \tag{A5}$$

The resulting λ should be constrained to an angle within a single orbit (i.e., $0 \leq \lambda \leq 2\pi$).

Appendix B: Calculating Temperature and Pressure Dependencies

The four variables used to calculate the water-to-energy conversion factor, E_{con}, given in Eq. 19 have temperature and/or pressure dependencies that may be solved using the equations presented here.

The temperature-dependent equation for the slope of the saturation vapor pressure-temperature curve, s, can be expressed as (Allen et al., 1998):

$$s = \frac{2.503 \times 10^6 \, \exp\left(\frac{17.27\, T_{air}}{T_{air}+237.3}\right)}{\left(T_{air}+237.3\right)^2}, \tag{B1}$$

where s ranges from about 11 to 393 $\mathrm{Pa\,K^{-1}}$ for T_{air} between -20 and $40\ ^\circ\mathrm{C}$. Please be aware of a typographical error in this formula as presented in Eq. 7 of Gallego-Sala et al. (2010).

The temperature-dependent equation for the latent heat of vaporization, L_v, may be expressed as (Henderson-Sellers, 1984):

$$L_v = 1.91846 \times 10^6 \left[\frac{T_{air}+273.15}{\left(T_{air}+273.15\right)-33.91}\right]^2, \tag{B2}$$

where L_v ranges from about 2.558×10^6 to 2.413×10^6 $\mathrm{J\,K^{-1}}$ for T_{air} between -20 and $40\ ^\circ\mathrm{C}$.

The temperature and pressure dependence of the density of water, ρ_w, may be expressed as (Chen et al., 1977):

$$\rho_w = \rho_o \, \frac{K_o + C_A\, P^*_{atm} + C_B\, {P^*_{atm}}^2}{K_o + C_A\, P^*_{atm} + C_B\, {P^*_{atm}}^2 - P^*_{atm}}, \tag{B3}$$

where ρ_o ($\mathrm{kg\,m^{-3}}$) is the density of water at 1 atm, K_o (bar) is the bulk modulus of water at 1 atm, C_A (unitless) and C_B ($\mathrm{bar^{-1}}$) are temperature-dependent coefficients, and P^*_{atm} (bar) is the atmospheric pressure (i.e., $1\ \mathrm{Pa} = 1 \times 10^{-5}$ bar).

The equation for ρ_o is based on the work of Kell (1975):

$$\rho_o = \sum_{i=0}^{8} C_i \, {T_{air}}^i. \tag{B4}$$

The equation for K_o is also based on the work of Kell (1975):

$$K_o = \sum_{i=0}^{5} C_i \, {T_{air}}^i. \tag{B5}$$

The equations for C_A and C_B are given as (Chen et al., 1977):

$$C_A = \sum_{i=0}^{4} C_i \, {T_{air}}^i, \tag{B6}$$

Geosci. Model Dev. Discuss., doi:10.5194/gmd-2016-49, 2016
Manuscript under review for journal Geosci. Model Dev.
Published: 15 April 2016

Geoscientific Model Development Discussions
Open Access
EGU

$$C_B = \sum_{i=0}^{4} C_i \, {T_{air}}^i. \tag{B7}$$

The coefficients for T_{air} in Eqns. B4 through B7 are given in Table 3.

The temperature and pressure dependence of the psychrometric constant, γ, may be expressed as (Allen et al., 1998):

$$\gamma = \frac{C_p \, M_a \, P_{atm}}{M_v \, L_v}, \tag{B8}$$

where C_p ($\mathrm{J\,kg^{-1}\,K^{-1}}$) is the temperature-dependent specific heat capacity of humid air; M_a ($\mathrm{kg\,mol^{-1}}$) and M_v ($\mathrm{kg\,mol^{-1}}$) are the molecular weights of dry air and water vapor, respectively; L_v ($\mathrm{J\,kg^{-1}}$) is the latent heat of vaporization of water; and P_{atm} (Pa) is the atmospheric pressure. Constants for M_a and M_v are given in Table 2. The temperature dependence of C_p may be assumed negligible (e.g., $C_p = 1.013 \times 10^3$ $\mathrm{J\,kg^{-1}\,K^{-1}}$) or calculated by (Tsilingiris, 2008):

$$C_p = \sum_{i=0}^{5} C_i \, {T_{air}}^i, \tag{B9}$$

where the coefficients of T_{air} are given in Table 3.

Author contributions. I. C. Prentice, M. T. Sykes, and W. Cramer developed the original model theory and methods. A. V. Gallego-Sala, B. J. Evans, H. Wang, and T. W. Davis contributed to model improvements. R. J. Whitley, B. D. Stocker, and T. W. Davis transcribed the new model code. The manuscript was prepared with contributions from all authors.

Acknowledgements. This work was primarily funded by Imperial College London as a part of the AXA Chair Programme on Biosphere and Climate Impacts. It is a contribution to the Imperial College initiative on Grand Challenges in Ecosystems and the Environment, and the ecosystem Modelling and Scaling infrasTructure (eMAST) facility of the Australian Terrestrial Ecosystem Research Network (TERN). TERN is supported by the Australian Government through the National Collaborative Research Infrastructure Strategy (NCRIS). BDS funded by the Swiss National Science Foundation (SNF) and the European Commission's 7th Framework Programme, under Grant Agreement number 282672, EMBRACE project. WC contributes to the Labex OT-Med (n° ANR-11-LABX-0061) funded by the French government through the A∗MIDEX project (n° ANR-11-IDEX-0001-02). AGS has been supported by a Natural Environment Research Council grant (NERC grant number NE/I012915/1).

Geosci. Model Dev. Discuss., doi:10.5194/gmd-2016-49, 2016
Manuscript under review for journal Geosci. Model Dev.
Published: 15 April 2016

References

Allen, C. W.: Astrophysical Quantities, The Athlone Press, London, 3rd edn., 1973.

Allen, R. G.: Assessing integrity of weather data for reference evapotranspiration estimation, J. Irrig. Drain. Div., 122, 97–106, 1996.

Allen, R. G., Pereira, L. S., Raes, D., and Smith, M.: FAO Irrigation and Drainage Paper No. 56, Tech. rep., Food and Agriculture Organization of the United Nations, Rome, Italy, 1998.

Berberan-Santos, M. N., Bodunov, E. N., and Pogliani, L.: On the barometric formula, Am. J. Phys., 65, 404–412, 1997.

Berger, A. L.: Long-term variations of daily insolation and quaternary climatic changes, J. Atmos. Sci., 35, 2362–2367, 1978.

Berger, A. L. and Loutre, M. F.: Insolation values for the climate of the last 10 million years, Quat. Sci. Rev., 10, 297–317, 1991.

Berger, A. L., Loutre, M. F., and Tricot, C.: Insolation and earth's orbital periods, J. Geophys. Res., 98, 10 341–10 362, 1993.

Budyko, M. I.: The heat balance of the earth's surface, Sov. Geogr., 2, 3–13, 1961.

Chen, C.-T., Fine, R. A., and Millero, F. J.: The equation of state of pure water determined from sound speeds, J. Chem. Phys., 66, 2142–2144, 1977.

Cooper, P. I.: The absorption of radiation in solar stills, Sol. Energy, 12, 333–346, 1969.

Cramer, W. and Prentice, I. C.: Simulation of regional soil moisture deficits on a European scale, Norsk geogr. Tidsskr. – Norwegian J. Geogr., 42, 149–151, 1988.

Cramer, W., Bondeau, A., Woodward, F. I., Prentice, I. C., Betts, R. A., Brovkin, V., Cox, P. M., Fisher, V., Foley, J. A., Friend, A. D., Kucharik, C., Lomas, M. R., Ramankutty, N., Sitch, S., Smith, B., White, A., and Young-Molling, C.: Global response of terrestrial ecosystem structure and function to CO_2 and climate change: results from six dynamic global vegetation models, Glob. Change Biol., 7, 357–373, doi:10.1046/j.1365-2486.2001.00383.x, 2001.

Dewitte, S., Crommelynck, D., Mekaoui, S., and Joukoff, A.: Measurement and uncertainty of the long-term total solar irradiance trend, Sol. Phys., 224, 209–216, 2004.

Doorenbos, J. and Pruitt, W. O.: FAO Irrigation and Drainage Paper No. 24, Tech. rep., Food and Agriculture Organization of the United Nations, Rome, Italy, 1977.

Duffie, J. A. and Beckman, W. A.: Solar engineering of thermal processes, John Wiley and Sons, New Jersey, 4th edn., 2013.

Federer, C. A.: Spatial variation of net radiation, albedo and surface temperature of forests, J. Appl. Meteorol., 7, 789–795, 1968.

Federer, C. A.: Transpirational supply and demand: plant, soil, and atmospheric effects evaluated by simulation, Water Resour. Res., 18, 355–362, 1982.

Fisher, J. B., Huntzinger, D. N., Schwalm, C. R., and Sitch, S.: Modeling the terrestrial biosphere, Annu. Rev. Env. Resour., 39, 91–123, doi:10.1146/annurev-environ-012913-093456, 2014.

Fröhlich, C.: Solar irradiance variability since 1978: Revision of the PMOD composite during solar cycle 21, Space Sci. Rev., 125, 53–65, 2006.

Gallego-Sala, A. V. and Prentice, I. C.: Blanket peat biome endangered by climate change, Nat. Clim. Ch., 3, 152–155, doi:10.1038/nclimate1672, 2012.

Gallego-Sala, A. V., Clark, J. M., House, J. I., Orr, H. G., Prentice, I. C., Smith, P., Farewell, T., and Chapman, S. J.: Bioclimatic envelope model of climate change impacts on blanket peatland distribution in Great Britain, Clim. Res., 45, 151–162, doi:10.3354/cr00911, 2010.

Ge, S., Smith, R. G., Jacovides, C. P., Kramer, M. G., and Carruthers, R. I.: Dynamics of photosynthetic flux density (PPFD) and estimates in coastal northern California, Theor. Appl. Climatol., 105, 107–118, doi:10.1007/s00704-010-0368-6, 2011.

Geosci. Model Dev. Discuss., doi:10.5194/gmd-2016-49, 2016
Manuscript under review for journal Geosci. Model Dev.
Published: 15 April 2016

Harris, I., Jones, P. D., Osborn, T. J., and Lister, D. H.: Updated high-resolution grids of monthly climatic observations - the CRU TS3.10 Dataset, Int. J. Climatol., 34, 623–642, doi:10.1002/joc.3711, 2014.

Harrison, S. P., Prentice, I. C., Barboni, D., Kohfeld, K. E., Ni, J., and Sutra, J.-P.: Ecophysiological and bioclimatic foundations for a global plant functional classification, J. Veg. Sci., 21, 300–317, doi:10.1111/j.1654-1103.2009.01144.x, 2010.

Haxeltine, A. and Prentice, I. C.: BIOME3: An equilibrium terrestrial biosphere model based on ecophysiological constraints, resource availability, and competition among plant functional types, Global Biogeochem. Cycles, 10, 693–709, 1996.

Henderson-Sellers, B.: A new formula for latent heat of vaporization of water as a function of temperature, Q. J. R. Meteorol. Soc., 110, 1186–1190, 1984.

Hulme, D., Conway, D., Jones, P. D., Jiang, T., Barrow, E. M., and Turney, C.: Construction of a 1961–1990 European climatology for climate change modelling and impact applications, Int. J. Climatol., 15, 1333–1363, 1995.

Kaplan, J. O.: Geophysical Applications of Vegetation Modeling, Ph.D. thesis, Lund University, Lund, 2001.

Kell, G. S.: Density, thermal expansivity, and compressibility of liquid water from 0° to 150°C: Correlations and tables for atmospheric pressure and saturation reviewed and expressed on 1968 temperature scale, J. Chem. Eng. Data, 20, 97–105, 1975.

Knorr, W. and Heimann, M.: Impact of drought stress and other factors on seasonal land biosphere CO_2 exchange studied through an atmospheric tracer transport model, Tellus, 47B, 471–489, 1995.

Kopp, G. and Lean, J. L.: A new, lower value of total solar irradiance: Evidence and climate significance, Geophys. Res. Lett., 38, doi:10.1029/2010GL045777, 2011.

Lhomme, J.-P.: A theoretical basis for the Priestley-Taylor coefficient, Bound.-Lay. Meteorol., 82, 179–191, 1997.

Linacre, E. T.: Further studies of the heat transfer from a leaf, Plant Physiol., 42, 651–658, 1967.

Linacre, E. T.: Estimating the net-radiation flux, Agr. Meteorol., 5, 49–63, 1968.

McCree, K. J.: Test of current definitions of photosynthetically active radiation against leaf photosynthesis data, Agr. Meteorol., 10, 443–453, 1972.

Meek, D. W., Hatfield, J. L., Howell, T. A., Idso, S. B., and Reginato, R. J.: A generalized relationship between photosynthetically active radiation and solar radiation, Agron. J., 76, 939–945, 1984.

Meng, T.-T., Wang, H., Harrison, S. P., Prentice, I. C., Ni, J., and Wang, G.: Responses of leaf traits to climatic gradients: adaptive variation versus compositional shifts, Biogeosciences, 12, 5339–5352, doi:10.5194/bg-12-5339-2015, 2015.

Middleton, N. and Thomas, D., eds.: World Atlas of Desertification, John Wiley and Sons, Inc., New York, 2nd edn., 1997.

Moldover, M. R., Trusler, J. P. M., Edwards, T. J., Mehl, J. B., and Davis, R. S.: Measurement of the universal gas constant R using a spherical acoustic resonator, J. Res. Natl. Bur. Stand., 93, 85–144, 1988.

Monteith, J. L.: Symposia of the Society for Experimental Biology, vol. 19, chap. Evaporation and environment, pp. 205–234, Academic Press, Inc., New York, 1965.

Monteith, J. L. and Unsworth, M. H.: Principles of Environmental Physics, Butterworth-Heinemann, Oxford, 2nd edn., 1990.

New, M., Hulme, M., and Jones, P.: Representing twentieth-century space-time climate variability. Part I: Development of a 1961–90 mean monthly terrestrial climatology, J. Clim., 12, 829–856, 1999.

Penman, H. L.: Natural evaporation from open water, bare soil and grass, Proc. R. Soc. Lond. A, 193, 120–145, doi:10.1098/rspa.1948.0037, 1948.

Prentice, I. C. and Cowling: Encyclopedia of Biodiversity, chap. Dynamic global vegetation models, pp. 607–689, Academic Press, Inc., Waltham, 2nd edn., 2013.

Prentice, I. C., Cramer, W., Harrison, S. P., Leemans, R., Monserud, R. A., and Solomon, A. M.: A global biome model based on plant physiology and dominance, soil properties and climate, J. Biogeogr., 19, 117–134, 1992.

Prentice, I. C., Sykes, M. T., and Cramer, W.: A simulation model for the transient effects of climate change on forest landscapes, Ecol. Modell., 65, 51–70, 1993.

Prentice, I. C., Liang, X., Medlyn, B. E., and Wang, Y.-P.: Reliable, robust and realistic: the three R's of next-generation land-surface modelling, Atmos. Chem. Phys. Discuss., 14, 24 811–24 861, doi:10.5194/acpd-14-24811-2014, 2014.

Priestley, C. H. B. and Taylor, R. J.: On the assessment of surface heat flux and evaporation using large-scale parameters, Mon. Weather Rev., 100, 81–92, 1972.

Quillet, A., Peng, C., and Garneau, M.: Toward dynamic global vegetation models for simulating vegetation-climate interactions and feedbacks: recent developments, limitations, and future challenges, Environ. Rev., 18, 333–353, doi:10.1139/A10-016, 2010.

Raupach, M. R.: Equilibrium evaporation and the convective boundary layer, Bound.-Lay. Meteorol., 96, 107–141, 2000.

Raupach, M. R.: Combination theory and equilibrium evaporation, Q.J.R. Meteorol. Soc., 127, 1149–1181, doi:10.1002/qj.49712757402, 2001.

Sellers, P. J.: Canopy reflectance, photosynthesis and transpiration, Int. J. Remote Sens., 6, 1335–1372, doi:10.1080/01431168508948283, 1985.

Sitch, S., Smith, B., Prentice, I. C., Arneth, A., Bondeau, A., Cramer, W., Kaplan, J. O., Levis, S., Lucht, W., Sykes, M. T., Thonicke, K., and Venevsky, S.: Evaluation of ecosystem dynamics, plant geography and terrestrial carbon cycling in the LPJ dynamic global vegetation model, Glob. Change Biol., 9, 161–185, doi:10.1046/j.1365-2486.2003.00569.x, 2003.

Spencer, J. W.: Fourier series representation of the position of the sun, Search, 2, 172, 1971.

Stanhill, G. and Fuchs, M.: The relative flux density of photosynthetically active radiation, J. Appl. Ecol., 14, 317–322, 1977.

Stephenson, N. L.: Actual evapotranspiration and deficit: biologically meaningful correlates of vegetation distribution across spatial scales, J. Biogeogr., 25, 855–870, 1998.

Swift, Jr., L. W.: Algorithm for solar radiation on mountain slopes, Water Resour. Res., 12, 108–112, 1976.

Sykes, M. T. and Prentice, I. C.: Boreal forest futures: modelling the controls on tree species range limits and transient responses to climate change, Water, Air, Soil Pollut., 82, 415–428, 1995.

Sykes, M. T. and Prentice, I. C.: Climate change, tree species distributions and forest dynamics: a case study in the mixed conifer/northern hardwoods zone of Northern Europe, Clim. Change, 34, 161–177, 1996.

Sykes, M. T., Prentice, I. C., and Cramer, W.: A bioclimatic model for the potential distributions of north European tree species under present and future climates, J. Biogeogr., 23, 203–233, 1996.

Thekaekara, M. P. and Drummond, A. J.: Standard values for the solar constant and its spectral components, Nature, Phys. Sci., 229, 6–9, 1971.

Thornthwaite, C. W.: An approach toward a rational classification of climate, Geogr. Rev., 38, 55–94, 1948.

Tsilingiris, P. T.: Thermophysical and transport properties of humid air at temperature range between 0 and 100 °C, Energy Convers. Manage., 49, 1098–1110, 2008.

Ukkola, A. M., Prentice, I. C., Keenan, T. F., van Dijk, A. I. J. M., Viney, N. R., Myneni, R. B., and Bi, J.: Reduced streamflow in water-stressed climates consistent with CO_2 effects on vegetation, Nat. Clim. Change, doi:10.1038/nclimate2831, 2015.

Wang, H., Prentice, I. C., and Davis, T. W.: Biophysical constraints on gross primary production by the terrestrial biosphere, Biogeosciences, 11, 5987–6001, doi:10.5194/bg-11-5987-2014, 2014.

Geosci. Model Dev. Discuss., doi:10.5194/gmd-2016-49, 2016
Manuscript under review for journal Geosci. Model Dev.
Published: 15 April 2016

Weedon, G. P., Balsamo, G., Bellouin, N., Gomes, S., Best, M. J., and Viterbo, P.: The WFDEI meteorological forcing data set: WATCH Forcing Data methodology applied to ERA-Interim reanalysis data, Water Resour. Res., 50, 7505–7514, doi:10.1002/2014WR015638, 2014.

Willson, R. C.: Total solar irradiance trend during solar cycles 21 and 22, Science, 277, 1963–1965, 1997.

Woodward, F. I. and Lomas, M. R.: Vegetation dynamics—simulating responses to climatic change, Biol. Rev., 79, 643–670, doi:10.1017/S1464793103006419, 2004.

Woolf, H. M.: On the computation of solar evaluation angles and the determination of sunrise and sunset times, Tech. Rep. NASA-TM-X-164, National Aeronautics and Space Administration, Washington, DC, 1968.

Geosci. Model Dev. Discuss., doi:10.5194/gmd-2016-49, 2016
Manuscript under review for journal Geosci. Model Dev.
Published: 15 April 2016

Geoscientific Model Development Discussions
Open Access
EGU

Table 1. Nomenclature.

Instantaneous	
S_w	evaporative supply rate, $\mathrm{mm\,h^{-1}}$
D_p	evaporative demand rate, $\mathrm{mm\,h^{-1}}$
E^q	equilibrium evapotranspiration rate, $\mathrm{mm\,h^{-1}}$
E^p	potential evapotranspiration rate, $\mathrm{mm\,h^{-1}}$
E^a	actual evapotranspiration rate, $\mathrm{mm\,h^{-1}}$
I_o	extraterrestrial solar radiation flux, $\mathrm{W\,m^{-2}}$
I_N	net radiation flux, $\mathrm{W\,m^{-2}}$
I_{SW}	net shortwave solar radiation flux, $\mathrm{W\,m^{-2}}$
I_{LW}	net longwave radiation flux, $\mathrm{W\,m^{-2}}$
Daily	
W_n	soil moisture, mm
P_n	precipitation, $\mathrm{mm\,d^{-1}}$
C_n	condensation, $\mathrm{mm\,d^{-1}}$
RO	runoff, mm
E_n^q	equilibrium evapotranspiration, $\mathrm{mm\,d^{-1}}$
E_n^p	potential evapotranspiration, $\mathrm{mm\,d^{-1}}$
E_n^a	actual evapotranspiration, $\mathrm{mm\,d^{-1}}$
H_o	solar irradiation, $\mathrm{J\,m^{-2}\,d^{-1}}$
H_N	net surface radiation, $\mathrm{J\,m^{-2}\,d^{-1}}$
H_N^*	nighttime net surface radiation, $\mathrm{J\,m^{-2}\,d^{-1}}$
Q_n	photosynthetically active radiation, $\mathrm{mol\,m^{-2}\,d^{-1}}$
S_f	fraction of bright sunshine hours, unitless
T_{air}	mean air temperature, $^\circ\mathrm{C}$
Monthly	
E_m^q	equilibrium evapotranspiration, $\mathrm{mm\,mo^{-1}}$
E_m^p	potential evapotranspiration, $\mathrm{mm\,mo^{-1}}$
E_m^a	actual evapotranspiration, $\mathrm{mm\,mo^{-1}}$
ΔE_m	climatic water deficit, $\mathrm{mm\,mo^{-1}}$
α_m	Priestley-Taylor coefficient, unitless

Geosci. Model Dev. Discuss., doi:10.5194/gmd-2016-49, 2016
Manuscript under review for journal Geosci. Model Dev.
Published: 15 April 2016

Geoscientific Model Development Discussions
Open Access
EGU

Table 1 (continued). Nomenclature.

Miscellaneous	
$\cos\theta_z$	inclination factor, unitless
δ	declination angle, rad
d_r	distance factor, unitless
ε	obliquity, rad
e	eccentricity, unitless
E_{con}	water to energy conversion factor, $\mathrm{m^3\,J^{-1}}$
γ	psychrometric constant, $\mathrm{Pa\,K^{-1}}$
h	hour angle, rad
h_i	intersection of evaporative rates hour angle, rad
h_n	net radiation crossover hour angle, rad
h_s	sunset hour angle, rad
i	day of month (1–31)
λ	true longitude, rad
L_v	latent heat of vaporization of water, $\mathrm{J\,kg^{-1}}$
ν	true anomaly, rad
n	day of year (i.e., 1–365)
N_a	total number of days in a year (e.g., 365)
N_m	total number of days in a given month (e.g., 31)
$\widetilde{\omega}$	longitude of perihelion, rad
ϕ	latitude, rad
P_{atm}	atmospheric pressure, Pa
ρ_w	density of water, $\mathrm{kg\,m^{-3}}$
r_u	$\sin\delta\ \sin\phi$, unitless
r_v	$\cos\delta\ \cos\phi$, unitless
r_w	$(1-\beta_{sw})\ \tau\ I_{sc}\ d_r$, $\mathrm{W\,m^{-2}}$
r_x	$3.6\times10^6\ (1+\omega)\ E_{con}$, $\mathrm{mm\,m^2\,W^{-1}\,h^{-1}}$
s	slope of saturated vapor pressure-temperature curve, $\mathrm{Pa\,K^{-1}}$
τ	transmittivity, unitless
τ_o	transmittivity at mean sea level, unitless
z	elevation above mean sea level, m

Geosci. Model Dev. Discuss., doi:10.5194/gmd-2016-49, 2016
Manuscript under review for journal Geosci. Model Dev.
Published: 15 April 2016

Geoscientific Model Development Discussions
Open Access
EGU

Table 2. Constants and Standard Values.

Variable	Units	Description
A	107 °C	empirical constant, Eq. 13 (Monteith and Unsworth, 1990)
β_{sw}	0.17	shortwave albedo, Eq. 10 (Federer, 1968)
β_{vis}	0.03	visible light albedo, Eq. 17 (Sellers, 1985)
b	0.20	empirical constant, Eq. 13 (Linacre, 1968)
c	0.25	cloudy transmittivity, Eq. 12 (Linacre, 1968)
d	0.50	angular coefficient of transmittivity, Eq. 12 (Linacre, 1968)
fFEC	2.04 µmol J^{-1}	flux-to-energy conversion, Eq. 17 (Meek et al., 1984)
g	9.80665 $m\,s^{-2}$	standard gravity, Eq. 20 (Allen, 1973)
I_{sc}	1360.8 $W\,m^{-2}$	solar constant, Eq. 2 (Kopp and Lean, 2011)
L	0.0065 $K\,m^{-1}$	mean adiabatic lapse rate, Eq. 20 (Allen, 1973)
M_a	0.028963 $kg\,mol^{-1}$	molecular weight of dry air, Eq. 20 (Tsilingiris, 2008)
M_v	0.01802 $kg\,mol^{-1}$	molecular weight of water vapor, Eq. B8 (Tsilingiris, 2008)
ω	0.26	entrainment factor, Eq. 22 (Priestley and Taylor, 1972)
P_o	101325 Pa	standard sea-level pressure, Eq. 20 (Allen, 1973)
R	8.31447 $J\,mol^{-1}\,K^{-1}$	universal gas constant, Eq. 20 (Moldover et al., 1988)
S_c	1.05 $mm\,h^{-1}$	supply rate constant, Eq. 21 (Federer, 1982)
T_o	288.15 K	base temperature, Eq. 20 (Berberan-Santos et al., 1997)
W_m	150 mm	soil moisture capacity, Eq. 21 (Cramer and Prentice, 1988)

Table 3. Coefficients of T_{air}.

	ρ_o ($kg\,m^{-3}$) Eq. B4	K_o (bar) Eq. B5	C_A (unitless) Eq. B6	C_B (bar^{-1}) Eq. B7	C_p ($J\,kg^{-1}\,K^{-1}$) Eq. B9
C_0	$+9.998395 \times 10^{2}$	$+1.96520 \times 10^{4}$	$+3.26138$	$+7.2061 \times 10^{-5}$	$+1.004571 \times 10^{3}$
C_1	$+6.78826 \times 10^{-2}$	$+1.48183 \times 10^{2}$	$+5.223 \times 10^{-4}$	-5.8948×10^{-6}	$+2.050633$
C_2	-9.08659×10^{-3}	-2.29995	$+1.324 \times 10^{-4}$	$+8.6990 \times 10^{-8}$	-1.631537×10^{-1}
C_3	$+1.02213 \times 10^{-4}$	$+1.28100 \times 10^{-2}$	-7.655×10^{-7}	-1.0100×10^{-9}	$+6.212300 \times 10^{-3}$
C_4	-1.35439×10^{-6}	-4.91564×10^{-5}	$+8.584 \times 10^{-10}$	$+4.3220 \times 10^{-12}$	-8.830479×10^{-5}
C_5	$+1.47115 \times 10^{-8}$	$+1.03553 \times 10^{-7}$	—	—	$+5.071307 \times 10^{-7}$
C_6	-1.11663×10^{-10}	—	—	—	—
C_7	$+5.04407 \times 10^{-13}$	—	—	—	—
C_8	-1.00659×10^{-15}	—	—	—	—